Techno-economic optimization of Concentrated Solar Power plants with thermocline thermal energy storage and integrated steam generator

Alberto Pizzolato[a], Vittorio Verda[a], Adriano Sciacovelli[a] and Filippo Donato[b]

[a] Politecnico di Torino, Turin, Italy, alberto@pizzolato polito.it, vittorio.verda@polito.it, adriano.sciacovelli@polito.it
[b] ENEA, Rome, Italy, filippo.donato@enea.it

Abstract:

The utilization of molten salts as the Heat Transfer Fluid (HTF) in Concentrated Solar Power (CSP) allows to increase the maximum operational temperature of parabolic trough power plants, with a substantial gain in the power cycle efficiency. ENEA has recently tested a way to further ameliorate this concept by introducing a single-tank configuration of the storage system with an integrated steam generator, which can dramatically reduce the total investment cost and simplify the power plant layout. In this paper we propose to couple this system to a waste-heat recovery unit for the cogeneration of power, heating and cooling, which has the potential to extend the range of applications of CSP plants to small-size systems and to regions with a moderate solar resource. In this paper, a techno-economic analysis is implemented to investigate the feasibility of this innovative technological pathway, to determine the optimal design of a representative 1 MW_e plant located in Rome and to analyze its performances. Results reveal that the heat market brings a 28 % reduction of the Levelized Electricity Cost, allowing to reach the competitive value of 230.25 $/MWh. This is remarkably lower than the Feed-In-Tariff (FIT) of the Italian incentive scheme for CSP and comparable to the specific cost of larger plants despite an investment cost limited to 14.56 M$.

Keywords:

Concentrated Solar Power, Molten Salts, Solar Trigeneration, Thermocline Thermal Energy Storage, Techno-economic Optimization

1. Introduction

Concentrated Solar Power (CSP) has distinguished among other renewable technologies for the natural integration of a thermal storage system, which makes a highly fluctuating resource dispatchable on-demand. Unfortunately, the Levelized Electricity Cost (LEC) and the overnight construction cost of CSP remains hardly competitive with conventional fossil-based power plants. According to Ref. [1], the high upfront investment cost and the difficult siting are the two major barriers to a rising share of CSP in the future energy mix. It is clear that, in order to increase the penetration of the technology, greater research effort should aim at boosting the competitiveness of small CSP plants at the moderate latitudes.

The first step in this direction is acknowledged to be the simplification of the power plant loop through the reduction of the number of components. In this regard, ENEA (Italian National Agency for New Technologies, Energy and Sustainable Economic Development) has promoted [2] the use of a thermocline (i.e. single-tank) Thermal Energy Storage (TES) with an integrated Steam Generator (SG) submerged in the Heat Storage Medium. The plant can be further simplified through the use of the molten salts mixture, which was commonly found as Heat Storage Medium, also as the Heat Transfer Fluid [3] also with consistent benefits to the efficiency of the power cycle. A second field of competitiveness improvement for small CSP is represented by the polygeneration possibility. The option of CSP-driven desalination has been widely investigated [4, 5], since regions with high water scarcity generally have a large solar resource. Another interesting cogeneration option that is worth of mention is the CSP-driven biomass gasification, which has lately received

considerable attention in the scientific community [6]. On the other hand, it should be noted that only a few studies [7, 8] have investigated the cogeneration of power, heating and cooling in a single CSP plant, which could be an ideal opportunity to enlarge the market of CSP to users like small districts, university campuses and hospitals.

The innovative coupling of these two concepts, i.e. the ENEA compact system and the cogeneration option, has the potential to open the doors of CSP applications to small-scale facilities in regions with moderate solar resource. Nevertheless, little has been done to investigate the real feasibility of the whole conversion chain. In this respect, the utilization of the tools of energy, exergy and and economic analysis for the optimization of CSP plants was shown to be a very effective way to investigate the viability of innovative pathways and propose a conceptual design of novel systems. As a matter of fact, it has been proficiently applied to solar tower combined cycle [9, 10], parabolic through plants for process heat generation [11] and to CSP desalination plants [12]. However, to the knowledge of the authors, there are no studies focused on the optimization of CSP plant designed following the ENEA concept. Additionally, the techno-economic performance of this type of system has never been accurately determine to assess its real market potentials.

Hence, the objective of this paper is to simultaneously fill these literature gaps, i.e. to use the tools of techno-economic analysis to build a complete model of Concentrated Solar plants with thermocline TES and integrated steam generator, to evaluate the economic potential of a cogeneration option, to establish optimal design trends and to critically analyze its performances**.**

2. The CSP cogeneration plant with thermocline TES and integrated Steam Generator

The system recently proposed by ENEA is presented in Figure 1. Thanks to the molten salts pump (MSP), the "solar salt" (i.e. a eutectic mixture with 60 wt % $NaNO_3$ and 40 wt % KNO_3) is circulated from the storage tank into the receiver tubes. Two different concentrating technologies can be used, namely the Parabolic Trough Solar Collectors (PTSC) and the Linear Fresnel Solar Collectors (LFSC), without requiring large modifications to the rest of the system. Once the fluid has reached the desired temperature (normally around 550 °C), it is circulated back to the storage tank. If the system conditions do not allow to reach the desired maximum temperature the salts can be circulated back to the solar collectors with a by-pass valve. This is particularly common during the morning startup of the plant. The storage tank contains a steam generator, which is immersed in the molten salts. This sub-system is called Storage Tank with Integrated Steam Generator and labelled as STISG in the figure. The steam produced flows to the steam turbine and it is eventually condensed in the condenser (WCD). In cogeneration mode, the available thermal power collected by the cooling water in the steam condenser can be used to directly satisfy the thermal requirements of a heat consumer or can be fed to an Absorption Chiller Unit (ACU) in order to satisfy a cooling load. The temperature level required by the waste heat recovery unit has been set equal to 90 °C, in order to cope with the stringent requirements of the ACU. Finally, the Rankine cycle is closed with the use of a water pump (WP1).

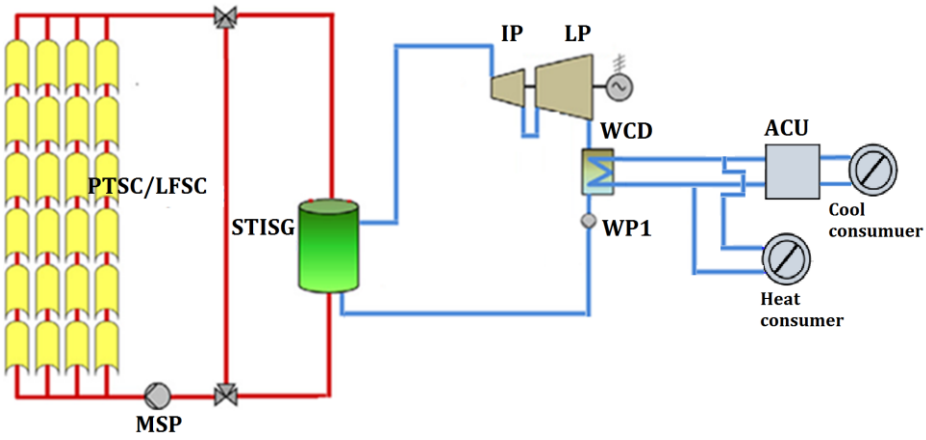

Figure 1. Proposed system layout

In the following sections, a summary of the modelling approach of the three main subsystems of the plant is given, namely the solar field, the STISG and the power block. On the other hand, the performance of the waste heat recovery unit has not been modelled accurately but calculated by setting the efficiency of the heat distribution system to 90 % and the Coefficient of Performance of the absorption chiller to 60 %. In fact, as clarified in the introductory section, cogeneration is here evaluated only in terms of economic potential and the detailed exergetic analysis of the byproduct generation system is not part of the objectives of the present work.

3. Models of power plant components

To simulate and predict the behaviour of the whole plant, the component models have been coded in MATLAB^{R} environment following an object-oriented technique. The component is thus represented by an instance of a particular class (i.e. an object), which contains all the phenomenological equations and is able to communicate signals, i.e. variables such as thermodynamic states, to the other components models to compute the performances across the entire system layout. Before the final assembling, the model of each component has been successfully validated with experimental data gathered at the ENEA research facility of La Casaccia, Rome. However, due to space constraints, in the present paper we will limit our treatment to the main governing equations and the interested reader is advised to examine the cited references for a more detailed understanding.

3.1. Modelling the solar field

The concentrating and receiver technologies considered in this study are the ones already in operation in the 5 MW Archimede plant of Priolo Gargallo [13], which are object of continuous experimental campaigns at the ENEA research centre.

The parabolic through reflector is a 12.5 m long parabolic mirror with 5.76 m of aperture and a focal height of 2.01 m. It sustains a 4.06 m long receiver tube consisting of an absorber inside a glass envelope with bellows at either end. The absorber is a stainless steel tube (70 mm in diameter) which is treated with selective coating to obtain a high absorptance in the solar energy spectrum, and low emittance in the infrared (i.e. 95 % and 7.3 % respectively from manufacturer specifications). The glass envelope (125 mm in diameter) is made of Pyrex and guarantees a transmittance higher than 96 % in the full range of operating temperatures. The annulus space between the absorber and the glass envelope is under vacuum (1 x 10^{-4} mbar) to reduce thermal losses.

In present work, simple analytical relationship available in literature [14] were used for the solar position and the optical model of the receiver while a slightly more complicated approach was followed for the thermal model of the receiver tube. In this latter case, a quasi 1D model was implemented: the receiver was discretized along the axial direction and, for each of the portion, a

thermal balance is written considering only non-advective heat transfer in the radial direction. This approach is widely used for the simulation of thermal systems of this type [14, 15].

In particular, we followed the formulation presented in [15] assuming steady state and for a negligible change in potential energy:

$$\dot{Q}_{net} = \dot{m}_{HTF}\left(h_{in} + e_{in} - h_{out} - e_{out}\right) \quad (1)$$

The term on the left hand side, namely $\dot{Q}_{net}$, is the radiative power that is effectively transferred to the heat transfer fluid and can be calculated as:

$$\dot{Q}_{net} = \dot{Q}_{abs} - \dot{Q}_{losses} \quad (2)$$

which is a difference between the concentrated solar power absorbed by the receiver $\dot{Q}_{abs}$ and the thermal losses of the receiver towards the environment $\dot{Q}_{losses}$. In steady-state conditions, the concentrated radiation absorbed on the surface of the absorber tube can be either transmitted to the Heat Transfer Fluid or rejected towards the environment. In the first case, we have a series of the following thermal resistance ((Fig. 2 [15]).):

- Conduction from the outer surface of the absorber tube to the inner surface of the absorber tube
- Convection from the inner surface of the absorber tube the heat transfer fluid

In the second case, the thermal power path is the following ((Fig. 2 [15]).):

- Radiation/convection heat transfer from the outer surface of the absorber tube to the inner surface of the glass envelope
- Conduction heat transfer across the glass envelope
- Radiation/convection heat transfer from the external surface of the glass envelope towards the environment

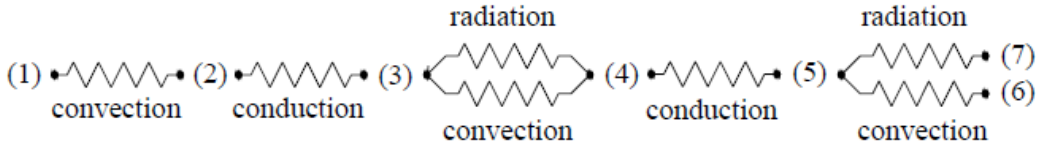

Figure 2. Electrical analogy for the radial heat transfer path in the receiver tube. (1) Heat Transfer Fluid, (2) absorber inner surface, (3) absorber outer surface, (4) glass envelope inner surface, (5) glass envelope outer surface, (6) air, (7) sky.

The thermal properties of the materials, as well as the correlations used for the calculation of the heat transfer coefficients have been maintained unchanged with respect to the ones proposed in [15]. As far as the weather data mining is concerned, the irradiance data were obtained from the HelioClim3 database and the wind speed and ambient temperature data from the EnergyPlus database, both making available weather data of 2005 with a 15 min sampling. The chosen location for the present study is Rome, 41°54′N 12°30′E. For such a location we found a total direct normal insolation available of 1790 KWh/(m^{2}year) and an average wind speed at the receiver tube level of 2.3 m/s.

3.2. Modelling the thermocline tank with integrated steam generator

The modelling of the integrated system is complicated by the nature of the physical phenomenon involved. The steam generator, in fact, is ruled by the laws of natural circulation on the molten salts side; this means that the salts mass flow is not fixed but depends upon the temperature profile of the liquid column inside the generator and the one of the undisturbed fluid in the storage tank. As a consequence, even if the two components of this subsystem, namely the steam generator and the storage tank, have been modelled separately, the overall solution should be reached simultaneously through an iterative approach.

The fluid temperatures along the axial dimension of the once-trough steam generator are calculated with a one-dimensional finite volume numerical model [16], where a double iteration is used to solve the natural circulation problem. The algorithm starts by guessing the outlet temperature of the molten salts and their mass flow rate. Then, the heat transfer equations are solved proceeding from the bottom to the top of the steam generator, the guessed temperature is corrected accordingly and the procedure repeated unless a satisfactory convergence is reached. In the latter case, the molten salts mass flow is corrected thanks to the fluid-dynamic model.

The calculation of the heat transfer coefficients has been performed using :

- The Dittus-Boelter correlation for the subcooled portion
- The Chen correlation [19] for the evaporating section
- The Heineman correlation [17] for the superheating section
- The correlation for helicoidal tube bundles for the molten salts side

Moving to the pressure drop on the molten salts side that rules the natural circulation in the steam generator, we have modelled it following Ref. [18].

As far as the modelling of the stratification in the TES is concerned, we have used the logistic distribution function to represent the non-dimensional molten salts temperature profile of a vertical fluid column inside the tank, as proposed in [20]. We have chosen to parameterize the function statistically, using 18 CFD simulations of a $k-\omega$ turbulent model. This approach was shown [20] to be extremely convenient for the adaptation of CFD results to annual system-level simulation and optimization

3.3 Modelling the power block

Recalling the system shown in Figure 1, the power block sub-system includes three main components, namely the steam turbine, the steam condenser and the feedwater pump.

The thermodynamic performance of the steam turbine was modelled according to the paper of Medina Flores [21]. The Authors proposed to write the isoentropic efficiency of the turbine as a function of the steam pressure level at the inlet and at the outlet section of the turbine. It is wise to highlight that the choice of the outlet pressure in a cogeneration system should be done considering the waste heat utilization strategy. For the sake of this work, the cooling water maximum temperature has been set to 90 °C. This choice is motivated by the fact that the heat rejected at the condenser should also be used during summer months to drive a single effect H_2O-LiBr absorption cooling machine.

In summary, the power output can be written as:

$$\dot{E}_{el} = \frac{1}{\beta}\left(\dot{m}\left(h_1 - h_{2,iso}\right) - \alpha\right) \tag{3}$$

Where α and β are two pressure-dependent fitting parameters calculated as proposed in [21]

An important addition we have made allows to account for transient operation still maintaining a low level of modeling complexity. According to Ref. [21], the power output of the turbines during the startup can be obtained through the use of a startup factor $F_{startup}$ in the following way:

$$\dot{E}_{el} = F_{startup}(t)\dot{E}_{nom} \tag{4}$$

The correction factor ranges from 0 to 1, at the beginning and at the end of the startup process respectively, and increase quadratically in time. It can be calculated with:

$$F_{startup}(t) = \left(\frac{t_{\sin ceStartup}(t)}{t_{startup}}\right)^2 \tag{5}$$

In the framework of this paper, $t_{startup}$ has been set to one hour.

As far as the condenser is concerned, the one considered in the present work is a shell and tube heat exchanger as the one described in Ref. [23]. The condenser axial coordinate has been discretized

and in each of the portion considered the thermal power $\dot{Q}$ is calculated by means of an energy balance.

The global heat transfer coefficient is determined as follows [23]:

$$U = \left(R_{fo} + \left(\frac{1}{h_i} + R_{fi} \right) \frac{d_o}{d_i} + \frac{t_w}{k_w} \frac{d_o}{D_m} + \frac{1}{h_0} \right)^{-1} \quad (6)$$

Here, R_f is the fouling factor, d is the diameter, t_w is the tube thickness, k_w is the tube conductivity and h is the heat transfer coefficient. Subscripts i and o apply for internal and external side of the tube respectively. D_m is mean diameter calculated as follows:

$$D_m = \frac{d_o - d_i}{\ln\left(\frac{d_o}{d_i} \right)} \quad (7)$$

This component is designed in order to ensure a minimum driving temperature difference, i.e. at the pinch point, equal to 10 °C. Considering the requirement of 90°C from the waste heat recovery unit and neglecting the subcooled portion of the heat exchanger, the steam condensing temperature was set to 100 °C:

Moving to the feedwater pump, the approach followed was advised by Pelster in Ref. [24] and is based on the following assumptions:

- Negligible kinetic and potential energy change across the component
- Negligible heat transfer towards the environment
- Internal dissipation determined by a priori-set pump hydraulic efficiency

Hence, the power consumption of the device $\dot{E}_{pump}$ can be calculated with:

$$\dot{E}_{pump} = \frac{1}{\eta_h} \dot{m}_{FW} \left(\frac{\Delta p}{\rho} \right) \quad (8)$$

Following the approach proposed by the same author, the pump outlet temperature T_{out} is computed as [24]:

$$T_{out} = T_{in} + \frac{(1 - \eta_h)\dot{E}_{pump}}{\dot{m}\bar{c}_p} \quad (9)$$

4. Techno-economic optimization

The genetic algorithm has been used in MATLAB® environment following a black-box approach. The optimizer and the model are coded separately and they exchange information during the optimization process in the form of decision variables and objective function. As required by the type of problem considered, a constraints block has to be added to avoid forbidden combinations of the objective functions, which are holes in the space of the solutions of the optimization problem.

As far as the Stopping Criteria (SC) are concerned, the single-objective genetic algorithm is stopped when the relative average best fitness function B change over the last N generations is less than 10^{-4}. In mathematical terms:

$$SC_i = \frac{\sum_{j=0}^{N-1} \left| B_{i-j} - B_{i-j-1} \right|}{N} \quad (10)$$

In the next section additional details about the choice of the decision variables and of the objective function are given.

4.1. Decision variables

Before any optimization can be performed, it is necessary to identify the design variables that the procedure can modify in order to reach the configuration with the best annual performance, namely

the decision variables. The ideal decision variable should have a large impact on the performance of the system and should practically correspond to a design-free parameter, i.e. a degree of freedom of the system designer.

All the decision variables used in the framework of the present work are presented in Table 1.

Table 1. Decision variables overview for the basic system optimization

Decision variable	**Lower bound**	**Upper bound**	**Type**
Number of hours of molten storage NH [hours]	2	24	Continuous
Tank aspect ratio D/H [-]	0.2	5	Continuous
Solar Multiple SM [-]	1	8	Continuous
Spacing between collectors $d_{spacing}$ [m]	5	25	Continuous
Steam generator height H [m]	1	4	Continuous
n. of tubes of the steam generator n_{tubes} [-]	3	10	Only integers
n. of collectors in a string n_{coll}[-]	2	8	Only integers
Tracking system axis [-]	1 = N-S	2: E-W	Only integers

The decision variables were selected in order to enhance freedom in the design of the TES, of the steam generator and of solar field. On the other hand, the power block is designed a priori to target an electrical capacity of 1 MW_{el}.

Starting from the TES system, the number of storage hours NH is an intuitive representation of the storage tank size. This value is the number of hours of continuous nominal operation that could be guaranteed to the power block during an ideal discharge process, i.e. starting from the tank fully charged at the maximum temperature and assuming no mixing during the discharge. Moreover, the aspect ratio of the tank is defined as the ratio of the tank diameter D to the tank height H. It is chosen in order to account the variability of the molten salts circulation and flow field that bring substantial changes in the rate of thermocline degradation.

Moving to the solar field, the solar multiple (SM) is a very well-known decision variable in the field of CSP technology. It is defined as the ratio of the total mirror area to the "exact mirror area". This last quantity is the solar field aperture area required to deliver to the power cycle the thermal power needed to operate the turbine in nominal conditions. Besides the total area, the optimal number of collectors per string n_{coll} should also be identified because this choice is expected to affect the solar field efficiency. In fact, the average mass flow rate that is circulated in the solar field is directly proportional to the total mirror area: although a higher mass flow rate means a higher heat transfer coefficient of the molten salts and thus a higher thermal performance, the pressure drop along the line increases and so does the power consumption of the molten salts pump. The optimal trade-off between these two trends should be found. Moreover, the orientation of the solar field is expected to play a major role on the annual performance of the system. The most common choice is either a solar field with the receiver axis aligned in the North-South (N-S) direction or in the East-West (E-W) direction. The optimizer can vary this variable between 1 and 2, being the former the N-S orientation and the latter the E-W orientation. Finally, the solar field design has one more degree of freedom, which is the solar field spacing $d_{spacing}$ between adjacent strings of solar collectors. A too compact solar field design can yield a high self-shadowing effect between solar collectors and a consequent drop in the optical efficiency. On the other hand, a too far placement implicates a higher land cost.

As far as the steam generator is concerned, two design variables have been identified, namely the number of tubes n_{tubes} and the height H. The bounds have been set according to some preliminary assessments performed by ENEA in the framework of the OPTS European project. Clearly, the number of tubes should be an integer value and an integer constraint has been implemented in the optimization routine.

4.2. Objective function

The objective function chosen for the present study is the Levelized Electricity Cost, which is representative of the potential profit of the proposed plant. The reduction of the exergoeconomic cost of the byproducts is out of the sake of this paper. which aims at driving down the specific cost of electricity only. Hence, as it will be clarified in this section, we calculated the cost of heat and cold flows a priori and subtracted the revenues linked to the sale of these byproducts on the market from the total annualized cost. In mathematical terms:

$$LEC = \frac{CRF \cdot C_{inv} + C_{O\&M} + C_{dec} + C_{cont} - R_{heat\&cold}}{E_y} \tag{11}$$

Where:

- CRF is the annualization factor that can be computed as:

  $$CRF = \frac{i(1+i)^n}{(1+i)^n - 1} + k_{ins} \tag{12}$$

  In the previous equation the interest i and insurance rate k_{ins} have been set to 7 % and 2 % respectively as suggested in Ref. [24].

- C_{inv} is the investment cost of the plant obtained summing the investment costs of all the components, i.e. $C_{inv} = \sum C_i$. The investment cost of the i^{eth} component C_i is calculated through the use of cost functions, which stem from a best-fit on a wide range of market data and relate the cost of component to a specific size parameter S_i. Mathematically [24]:

  $$C_i = c_{ref}\left(\frac{S_i}{S_{ref}}\right)^n f_{M\&S} \tag{13}$$

  The scale factor n keeps into consideration the economy of scale, i.e. smaller component specific cost is much higher than bigger components one. On the other hand, $f_{M\&S}$ is the Marshall and Swift equipment cost index ratio that keeps into account the evolution of equipment costs and it is used to allow a meaningful comparison between studies performed in different years. The adopted index for the present study is the one of 2011 obtained from Ref. [25] and set to 1546.5. The full reference data of c_{ref}, S_{ref}, and n for the power block is obtained by [24], while the ones related to the solar field and the molten salts TES are gathered from [26].

- $C_{O\&M}$ are the Operation & Maintanace costs. We have considered service contracts for groundkeeping, mirrors washing and water treatment, material maintenance for the equipment and operation cost due to personnel. All the data obtained through [26] have been normalized on the plant electrical capacity to obtain a specific O&M cost.

- C_{cont} and C_{dec} refer to contingencies costs and decommissioning costs. In the present paper we followed the approach presented in Ref. [24] and set them to 10 % and 5 % respectively of the total project cost.

- $R_{heat\&cold}$ accounts for the revenues from the heating and cooling market. In the framework of the present paper, thermal power is assumed to be completely sold to the user.to satisfy both heating (directly) and cooling needs (through the use of ACU). This income is used to conveniently decrease the specific cost of the main product, i.e. electricity, in order to extend benchmarking and allow comparison with only-electricity systems. In order to quantify these additional revenues, we have considered the savings brought by the CSP cogeneration installation with respect to a conventional natural gas boiler and a H20-LiBr absorption chiller. In mathematical terms:

$$R_{heat\&cold} = p_{NG}\left(\frac{Q_{heat} + \frac{Q_{cold}}{COP_{ACU}}}{\eta_{boiler}}\right) = p_{NG}\frac{Q_{wasteHeat}}{\eta_{boiler}} \quad (14)$$

Where the second equality sign holds thanks to the assumption of complete sale of the plant waste heat on the market. We have set the thermal efficiency of the typical natural gas boiler η_{boiler} to 90 %, and the price of natural gas p_{NG} equal to 10.087 €/GJ, that is the market price for industrial users in 2009 as set by the Italian Ministry of Development and Economic Resources

Table 2 has the aim to summarize the most relevant data implemented in the economic model. For a more exhaustive breakdown at the component level, the reader is advised to consult [16].

Table 2. Summary of economic model data

DIRECT COSTS	Cost	Unit	Scale factor	Reference size	Sources
Solar field	357	$/m^2	1	-	[26] & ENEA
Tank Envelope	2364	$/m^2	0.8	1909	[26]
Fluid, Foundations and Handling system (Tank)	1131	$/m^3	0.82	1060	[26] & ENEA
Steam Generator	11904	$/(n $_{tubes}$)	0.78	84	ENEA
Steam turbine	473	$/MW	0.67	25	[24]
Condenser	585	$/m^2	1	25	[24]
Pump, BOP, buildings, Safety systems(Power block)	376	$/MW	0.8	110	[26]
INDIRECT COSTS					
Engineering, Procurement, Construction & Project costs	11.8	% of direct capital cost	-	-	[26]
SERVICES and O&M					
Grounds/house keeping	0.04	$/m^2	-	-	Elaborated from [26]
Mirror washing	0.41	$/m^2	-	-	[26]
Water Treatment	1318	$/MW	-	-	[26]
Materials Maintenance	3.2	% of capital cost	-	-	[26]
TES and Power block Labor	5564	$/(MW y)	-	-	Elaborated from [26]
Solar field Labor	2.07	$/(m^2 y)	-	-	Elaborated from [26]
OTHER COSTS					
Contingencies	10	% of total project cost	-	-	[25]
Decommissioning	5	% of total project cost	-	-	[25]
Interest rate	7	%	-	-	[24]
Insurance rate	2	%	-	-	[24]

5. Results

5.1. Optimal design and performances

The specifications of the optimal design for the case presented are given in Table 2. The optimal design was obtained after 52 generations of 50 designs for a total of 2600 annual simulations.

It is worth noting that the optimal design presents quite a high value of solar multiple and storage tank size in order to increase the capacity factor of the steam turbine. However, the optimal storage tank size and solar multiple are far from the upper bound set for the optimization routine. This means that an optimum is present in the range considered and that the marginal cost of adding storage capacity and more mirrors to the solar field does not pay off.

On the other hand, the number of collectors per string is maximum which means that, in general, increasing the length of the single string results in a higher annual yield of the solar field. This result agrees with our intuition: in order to maintain fixed the salt temperature increase in the solar field a greater mass flow rate should be circulated in longer strings. Since the receiver tube cross section is constant, the consequence is an increase of the velocity of the HTF and ameliorate the internal heat transfer coefficient (and thus the receiver thermal efficiency). However, it should be noticed that, in ordinary operating conditions, a longer string implies higher thermal losses from nighttime circulation because molten salts circulates at a higher temperature to avoid freezing in the last part of the string. This phenomenon has been considered negligible in this paper and a more detailed investigation on this topic will be the subject of future studies.

The tank aspect ratio selected is quite in line with what is expected from some intuitive considerations. In fact, its choice is the trade-off between two competing phenomena and an optimal value is expected. A small tank aspect ratio brings a small average Reynolds number of the molten salts during the charging and discharging phase which reduces thermocline degradation due to turbulence. On the other hand, a large tank aspect ratio causes a reduction of time required to charge and discharge the system. However, also an enlargement of the thermocline is expected for large tank aspect ratio.

The height of the steam generator and the number of tubes selected are in close agreement with the detailed mechanical design proposed by the manufacturer for the European Project OPTS. Finally, the optimal tracking axis orientation for the case considered was found to be N-S. In fact, the annual electricity yield of the unit square meter of mirror is about 11 % higher compared to the E-W case for parabolic trough concentrators placed at the same latitude of Rome.

Table 3. Optimal design in the basic configuration

Hours of storage [-]	14.41
Tank Aspect ratio [-]	1.16
Solar multiple [-]	4.12
Mirror spacing [m]	15.23
Number of collectors per string [-]	8
Height of the steam generator [m]	2.58
Number of tubes of the steam generator [-]	9
Axis tracking	N-S

Table 3 summarizes the annual energy flows and the first law efficiencies. The proposed system in the optimal configuration generates 3864 MWh of electricity per year, which results in a capacity factor of the power block of 38.6 %.

It is wise to highlight that the optimal system waste no solar thermal energy. This means that all the solar energy collected by the HTF in the solar field is always fed to the storage and a situation of

complete charge never occurs. Furthermore, some reflections are necessary on the existence of an optimal capacity factor: if the designer wishes to reach 8760 Full Load Hours of the steam turbine, the solar field has to be oversized to run the power block 24 hours per day even in winter. Two possibilities, both unsatisfactory, are thus available to deal with this large amount of solar thermal energy:

- An oversized tank, whose complete volume would be unused for most of the year
- A normal tank, which would unable to store all the energy coming from the solar field in summer months thus resulting in a large amount of energy dumped

Table 4. Energy flows and efficiencies

Total power generation [MWh]	3864
Total heat sold [MWh]	10206
Total heat wasted [MWh]	0
Total auxiliaries [MWh]	117
Capacity Factor [%]	38.64
Power block efficiency [%]	25.41
Optical efficiency solar field [%]	48.55
Thermal efficiency solar field [%]	80.68
System gross electrical efficiency [%]	9.72
System net electrical efficiency [%]	9.45
System total efficiency [%]	38.44

A second-law analysis was also conducted to assess the performance of the plant in the optimal design; efficiencies of the selected components and relevant exergy flows are given in Table 4.

The exergy yield of the solar field is worse than what was calculated with the first-law analysis. In fact, the very low value exergetic efficiency of this subsystem is the result of a considerable amount of exergy destruction due to heat transfer. On the other hand, all the components downstream along the energy conversion chain are rather efficient from a second-law perspective. Consequently, this highlights once more the need of focusing future research on the components of the solar field.

Table 5. Exergy flows and 2nd law efficiencies

Yearly optical exergy losses [MWh]	19418
Yearly receiver exergy destruction due to heat transfer [MWh]	7369
Yearly receiver exergy losses [MWh]	2117
Yearly exergy losses for night-time circulation [MWh]	188
Yearly exergy destruction of the integrated storage system [MWh]	1262
Yearly steam turbine exergy destruction [MWh]	483
Yearly exergy destruction in the condenser [MWh]	4048
Yearly auxiliaries exergy utilization [MWh]	107
Exergetic Efficiency of concentrating device[%]	48.56
Exergetic Efficiency Receiver [%]	47.87
Exergetic Efficiency Storage [%]	83.48
Exergetic Efficiency Turbine [%]	87.50
Exergetic Efficiency Condenser [%]	84.63
Exergetic efficiency System [%]	16.08

Moving to the analysis of economic performances, the system requires a total capital investment of 14.56 million of US$ and can generate electrical power at the levelized cost of 230.25 US$/MWh. The CAPEX and LEC breakdown are represented in the pie charts of Figure 3. Results point out that the cost of the solar field is still the major factor of the total power plant investment cost accounting for 54 % of the total. The second largest item on the plant's owner expenditures list is the power block, which is accounts for 15 % of the total cost. Finally, the storage tank represents only 10 % of the total cost in the optimized configuration. The other pie chart represents the Levelized Electricity Cost breakdown where also the revenues generated from the heat sold on the market are included. In this way, it is possible to notice that cogeneration allows decreasing the specific cost of electricity of 28 % and this option is thus crucial for the economic viability of small CSP systems. On the real LEC (i.e. the one calculated without accounting for the revenues from the heat market) the annualized CAPEX are responsible of the 87 % of the total while the remaining part is due to Operation and Maintenance cost.

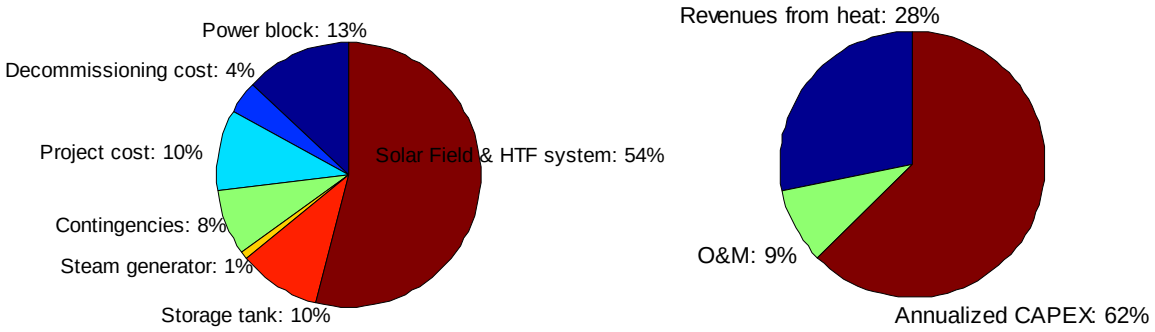

Figure 3. Left: Breakdown of the investment cost, Right: Breakdown of LEC

5.2. Sensitivity analysis

Due to great amount of time required for the algorithm convergence, a sensitivity analysis was conducted to simulate the performance of the system in the optimal configuration, whose details have been given in the previous section. A more accurate analysis would require the investigation of the trends of the optimal design with respect to the selected parameters. In fact, it is very likely that with different boundary conditions, i.e. different values of the fixed parameters, the optimal design will differ. In other words, we tested how the objective function value varies with respect to some parameters that were kept fixed in the optimization routine, namely the steam condensing temperature, the natural gas price and the components investment cost.

As can be understood from Figure 4a, the effect of decreasing the steam condensation temperature from the design value, i.e. 100 °C, has been found to be very limited. In fact, a reduction of 50°C of the condensation temperature, which should be connected with a waste heat utilization system able to deal with a lower temperature level, allows one to reduce the LEC of 20 $/MWh which represents only an 8 % improvement of the system in terms of objective function.

The natural gas price (Figure 4b) was set according to data gathered from the Italian Ministry of Economic Development. Such a value, as well as the price of all the conventional fuels, is expected to change in the future following policy-related trends. A 50 % increase of the natural gas price on the market, has the potential to bring the LEC down to 160 $/MWh. On the contrary, a 50 % abatement of the natural gas price can be very harmful to the economic feasibility of the system since the LEC is estimated to rise above 300 $/MWh.

As far as the components investment costs are concerned, only the effect of the storage tank and of the solar field were investigated (Figure 4b). In fact, since the power block design is based on a very mature technology, only small cost variations are expected to take place in the future. A 50 %

reduction of the solar field cost has the potential of halving the LEC and bringing it as low as 100 $/MWh, which is nearly competitive with conventional power plants. On the other hand, the storage tank cost is not expected to play a leading role in the development scenarios of the CSP technology since the system performance in the optimized configuration is slightly sensitive to large variations of the component cost. This observation will motivate our future research efforts in the modeling of a different concentrating device such as the Linear Fresnel Concentrators that, despite a lower degree of maturity, are considered a very promising technology.

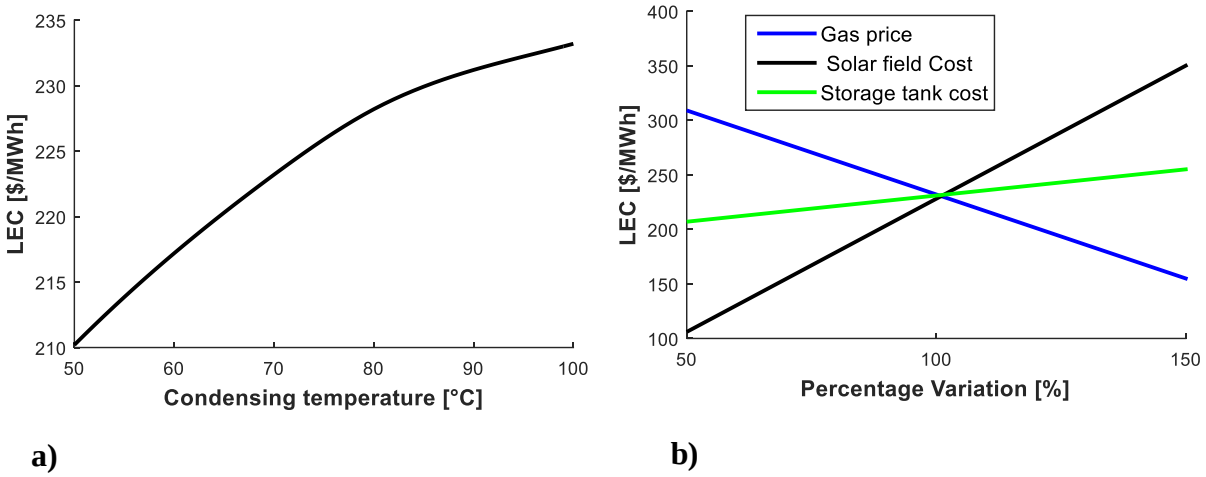

a) **b)**

Figure 4. Sensitivity analysis: LEC trend with respect to a) steam condensing temperature, b) Natural gas price, solar field investment cost and storage tank investment cost

6. Conclusions

The present study presents the techno-economic performances of CSP cogeneration plants with thermocline TES and integrated steam generator. We showed that such a solution can be economically convenient even at intermediate latitude and for small-scale systems, making the investment in CSP projects more attractive.

First of all, the single tank configuration with integrated steam generator is found to be particularly efficient (only 16 % of the incoming exergy is destroyed due to thermocline enlargement) and economically convenient, allowing to decrease the investment cost of storage technologies by roughly 41 %. Furthermore, according to our work the cogeneration mode is extremely important to drive down the specific cost of electricity. In fact, the increase of the steam condensing temperature marginally affects the electricity yield of the system but allows the recovery of a large amount of low-grade thermal energy for heating or cooling purposes. In this way, the Levelized Electricity Cost can be lowered of 28 % compared to the electricity-only configuration.

Additionally, it has been calculated that the optimal $1MW_e$ solar cogeneration plant located in Rome requires an initial investment of 14.56 MUS$ and can generate power at a price of 230.25 US$/MWh with a plant capacity factor of 38 %. Finally, the results highlights the need to focus future research on innovations of the solar field components, which accounts for 54 % of the total investment cost and is responsible of the destruction of 73 % of the incoming solar exergy flux.

Nomenclature

Letters

$\dot{E}$	Electrical power $[W]$	S	Characteristic size
$\dot{Q}$	Thermal power $[W]$	T	Temperature $[K]$
c_p	Specific Heat $\left[\frac{J}{kgK}\right]$	U	Global heat transfer coefficient $\left[\frac{W}{m^2K}\right]$

$f_{M\&S}$	Marshall & Swift cost index ratio $[-]$	d	Diameter $[m]$
$\dot{m}$	Mass flow rate $\left[\frac{kg}{s}\right]$	e	Specific kinetic energy $\left[\frac{J}{kg}\right]$
h	Specific enthalpy $\left[\frac{J}{kg}\right]$	n	Scale factor $[-]$
A	Area $[m^2]$	t	Time $[s]$
C	Cost [\$]	η	Efficiency $[-]$
L	Length $[m]$	ρ	Density $\left[\frac{kg}{m^3}\right]$

Subscripts

abs	Absorbed	i	Internal
dir	Direct	nom	Nominal
el	Electrical	ref	Reference
o	External	sol	Solar
FW	Feed-water	SF	Solar Field
f	Fouling	th	Thermal
HTF	Heat Transfer Fluid	$turb$	Turbine
h	Hydraulic	y	Yearly

References

[1] Lilliestam, J., Bielicki, J. M., & Patt, A. G. (2012). Comparing carbon capture and storage (CCS) with concentrating solar power (CSP): Potentials, costs, risks, and barriers. Energy policy, 47, 447-455.

[2] W. Gaggioli and L. Rinaldi, "An Innovative Concept of a Thermal Energy Storage (TES) System Based on the Single Tank Configuration Using Stratifying Molten Salts (MS) as both HSM and HTF, and with an Integrated Steam," in SolarPACES international Conference 2013, 2014, pp. 780–789.

[3] C. Rubbia, "Solar Thermal Energy production: guidelines and future programmes of ENEA" 2001.

[4] Palenzuela, P., Zaragoza, G., Alarcón, D., & Blanco, J. (2011). Simulation and evaluation of the coupling of desalination units to parabolic-trough solar power plants in the Mediterranean region. Desalination, 281, 379-387.

[5] Darwish, M. A., Abdul-Rahim, H., & Mohtar, R. (2012, October). Doha solar cogeneration power desalting pilot plant: Preliminary design. In Qatar Foundation Annual Research Forum (No. 2012).

[6] Ravaghi-Ardebili, Z., Manenti, F., Corbetta, M., Pirola, C., & Ranzi, E. (2015). Biomass gasification using low-temperature solar-driven steam supply. Renewable Energy, 74, 671-680.

[7] Al-Sulaiman, F. A., Hamdullahpur, F., & Dincer, I. (2012). Performance assessment of a novel system using parabolic trough solar collectors for combined cooling, heating, and power production. Renewable Energy, 48, 161-172.

[8] Buck, R., & Friedmann, S. (2007). Solar-assisted small solar tower trigeneration systems. Journal of Solar Energy Engineering, 129(4), 349-354.

[9] J. D. Spelling, "Hybrid Solar Gas-Turbine Power Plants A Thermoeconomic Analysis," Ph.D dissertation, Rotal Institute of Technology (KTH), Stockholm, 2013.

[10] Spelling, J., Favrat, D., Martin, A., & Augsburger, G. (2012). Thermoeconomic optimization of a combined-cycle solar tower power plant. Energy, 41(1), 113-120.

[11] Silva, R., Berenguel, M., Pérez, M., & Fernández-Garcia, A. (2014). Thermo-economic design optimization of parabolic trough solar plants for industrial process heat applications with memetic algorithms. Applied Energy, 113, 603-614.

[12] Fiorenza, G., Sharma, V. K., & Braccio, G. (2003). Techno-economic evaluation of a solar powered water desalination plant. Energy Conversion and Management, 44(14), 2217-2240.

[13] Falchetta, M., Gambarotta, A., Vaja, I., Cucumo, M., & Manfredi, C. (2006). Modelling and simulation of the thermo and fluid dynamics of the "Archimede Project" solar power station. In Proceedings of ECOS 2006.

[14] F. Zaversky, R. Medina, J. García-Barberena, M. Sánchez, and D. Astrain, "Object-oriented modeling for the transient performance simulation of parabolic trough collectors using molten salt as heat transfer fluid," Sol. Energy, vol. 95, pp. 192–215, Sep. 2013.

[15] R. Forristall, "Heat Transfer Analysis and Modeling of a Parabolic Trough Solar Receiver Implemented in Engineering Equation Solver Heat Transfer Analysis and Modeling of a Parabolic Trough Solar Receiver Implemented in Engineering Equation Solver," Tech. Report, Golden, Colorado, 2003.

[16] Pizzolato, A. (2014) "Thermoeconomic optimization of CSP plants with thermocline TES and integrated steam generator," MS Thesis, Politecnico di Torino, Turin

[17] Thulukkanam, K. (2013). Heat exchanger design handbook. CRC Press.

[18] Yu, W., France, D. M., Wambsganss, M. W., & Hull, J. R. (2002). Two-phase pressure drop, boiling heat transfer, and critical heat flux to water in a small-diameter horizontal tube. International Journal of Multiphase Flow, 28(6), 927-941.

[19] Chen, J. C. (1966). Correlation for boiling heat transfer to saturated fluids in convective flow. Industrial & Engineering Chemistry Process Design and Development, 5(3), 322-329

[20] Pizzolato, A., Donato, F., Verda, V., & Santarelli, M. (2015). CFD-based reduced model for the simulation of thermocline thermal energy storage systems. Applied Thermal Engineering, 76, 391-399.

[21] J. M. Medina-Flores and M. Picón-Núñez, "Modelling the power production of single and multiple extraction steam turbines," Chem. Eng. Sci., vol. 65, no. 9, pp. 2811–2820, May 2010.

[23] H. Hajabdollahi, P. Ahmadi, and I. Dincer, "Thermoeconomic optimization of a shell and tube condenser using both genetic algorithm and particle swarm," Int. J. Refrig., vol. 34, no. 4, pp. 1066–1076, Jun. 2011.

[24] S. Pelster, D. Favrat, and M. R. von Spakovsky, "The Thermoeconomic and Environomic Modeling and Optimization of the Synthesis, Design, and Operation of Combined Cycles With Advanced Options," J. Eng. Gas Turbines Power, vol. 123, no. 4, p. 717, 2001.

[25] M. Darwish, "Modular Hybridization of Solar Thermal Power Plants For Developing Nations," M.S. thesis, Royal Institute of Technology (KTH), Stockholm, 2012.

[26] Turchi, C. (2010). Parabolic trough reference plant for cost modeling with the solar advisor model (SAM) (No. NREL/TP-550-47605). National Renewable Energy Laboratory (NREL), Golden, CO.